Proceedings of the International Conference on Industrial Engineering and Operations Management

Publisher: IEOM Society International, USA DOI: 10.46254/IN05.20250479
Published: November 6, 2025

Comparative Study of TPMS Structure for Air Flow Resistivity and Mechanical Properties

Gomtesh Balaso Upadhye
School of Mechanical Engineering
Vellore Institute of Technology, Vellore
Vellore, Tamil Nadu, India
upadhye.gomtesh2024@vitstudent.ac.in

Gunji Bala Murali
School of Mechanical Engineering
Vellore Institute of Technology, Vellore
Vellore, Tamil Nadu, India
balamurali.g@vit.ac.in

Abstract

This study presents a systematic comparison of four triply periodic minimal surface (TPMS) structures—Gyroid, Diamond, Primitive, and I-WP—fabricated using stereolithography (SLA) for multifunctional engineering applications. Through comprehensive experimental evaluation of airflow resistivity and mechanical properties, we demonstrate how topological design governs critical performance trade-offs between fluid permeability and structural integrity. The specimens were characterized under controlled loading and flow conditions to assess stiffness, strength, and pressure drop behavior. Among the tested architectures, Diamond structures exhibit superior characteristics for applications requiring both efficient fluid flow and high load-bearing capacity due to their balanced curvature and robust nodal connectivity. Gyroid configurations show versatile and well-balanced multifunctional performance, making them suitable for systems that demand both mechanical stability and moderate permeability. In contrast, Primitive and I-WP structures display intermediate performance with distinct advantages for specialized applications such as acoustic damping or controlled ventilation. The results reveal that pore connectivity, wall thickness, and mean surface curvature critically influence airflow resistance, while structural hierarchy and periodic symmetry determine mechanical stability. These findings provide fundamental insights into structure–property relationships in TPMS lattices and establish practical guidelines for selecting optimal cellular architectures in thermal management systems, energy absorbers, and lightweight structural components. Overall, the study establishes a comprehensive framework for designing TPMS-based solutions that simultaneously optimize ventilation efficiency, energy dissipation, and mechanical performance in advanced engineering applications

Keywords
Airflow resistivity, Lattice structure, Triply periodic minimal surface, Additive manufacturing, Pressure drop.

1. Introduction
Triply Periodic Minimal Surface (TPMS) structures, which are three-dimensional minimal surfaces, are becoming increasingly popular in materials science and engineering due to their unique geometries, high mechanical efficiency, and potential for effective fluid transport. These surfaces, defined by their periodicity in three dimensions and zero mean curvature, offer an ideal framework for lightweight structures, optimized strength-to-weight ratios, and tailored porosity suitable for mass and heat transfer (Journal of Mines, Metals and Fuels, 2023). Originating from mathematical

models of minimal surfaces, TPMS geometries such as Gyroid, Diamond, I-WP, and Primitive have been recognized for their smooth, continuous surfaces and are widely applied in biomedical scaffolds, energy absorbers, filters, and acoustic materials (Poltue, T., Karuna, C., Khrueaduangkham, S., Seehanam, S., and Promoppatum, P. 2021).

Recent advancements in additive manufacturing, especially stereolithography (SLA), have made it possible to fabricate such complex geometries with high accuracy and surface quality (Catchpole-Smith, S., Aboulkhair, N., Clare, A., and Tuck, C. 2019) In this research, 36 TPMS specimens were fabricated using SLA, consisting of nine specimens for each of the Gyroid, Diamond, I-WP, and Primitive structures. These were evaluated through airflow resistivity and uniaxial compression tests to investigate the effect of topology on airflow resistance and mechanical behavior. The study aims to understand the relationship between surface curvature, pore connectivity, and load-bearing capacity to guide the design of multifunctional engineering components (Zhang, L., Feih, S., Daynes, S., Chang, S., Wang, M. Y., Wei, J., and Lu, W. F. 2018).

Conventional lattice or porous structures often suffer from stress concentration at junctions, non-uniform deformation, and inconsistent flow behavior under load (Sun, Q., Sun, J., Guo, K., and Wang, L. 2022). TPMS structures overcome these issues by offering a smooth, continuous, and interconnected architecture that promotes uniform stress distribution and tunable porosity. Their ability to balance structural stiffness and permeability makes them ideal candidates for applications in aerospace, biomedical, energy, and filtration systems where lightweight yet mechanically strong and fluid-permeable materials are required (Al-Ketan, O., Rowshan, R., and Abu Al-Rub, R. K. 2017). However, despite growing interest, systematic experimental comparisons of different TPMS topologies fabricated via SLA remain limited, particularly regarding their airflow resistivity and mechanical performance (Al-Ketan, O., and Abu Al-Rub, R. K. 2019).

Although TPMS structures are theoretically well-understood, there is a lack of comprehensive experimental data that correlates their topological features with multifunctional performance metrics such as permeability and compressive strength (Karcher, H. 1989). Existing studies often focus on single-property optimization, either mechanical or fluidic, without addressing the trade-offs between airflow resistance and load-bearing capability (Schwarz, H. A. 1865). Furthermore, most reported studies rely on metal-based additive processes like Selective Laser Melting (SLM) or Electron Beam Melting (EBM), leaving a gap in understanding the behavior of polymeric TPMS structures fabricated using SLA, which is known for its high resolution and smooth surface finish (Schoen, A. H. 1970). Therefore, there is a pressing need to experimentally evaluate and compare Gyroid, Diamond, Primitive, and I-WP topologies under identical manufacturing and testing conditions.

2. Methods

This paper provides an in-depth analysis of triply periodic minimal surfaces (TPMS), with a particular emphasis on the Gyroid, Diamond, I-WP, and Primitive geometries. By employing the stereolithography (SLA) technique, we created a total of 36 resin specimens, with nine specimens assigned to each TPMS configuration. The main goal of the study is to assess and compare the airflow resistivity and mechanical properties of these different structures. Each specimen was subjected to thorough testing, including airflow resistivity tests to measure their permeability and compression tests to evaluate their mechanical strength. This study seeks to uncover the connection between the shape and structure of TPMS and their performance characteristics, offering valuable knowledge for future material design and engineering endeavors.

To construct the TPMS (Triple Periodic Minimal Surface) structure, I started by developing a comprehensive 3D model in Creo, paying close attention to the precise parameters that determine its complex shape. After finalizing the design, I exported the model in the STL file format, which is commonly used for 3d printing. After importing the STL file into Chitu box software, I carried out the required slicing to prepare the model for the printing process. This involved adjusting the layer height, support structures, and other print settings to achieve the best possible outcome. After configuring the settings in the Chitu box, I proceeded to prepare the model for 3D printing, ensuring that the TPMS structure would meet the required precision and performance during the printing process. In this study, we focused on the design and fabrication of various lattice structures, specifically Gyroid, Diamond, Primitive, and I-WP, chosen for their distinctive mechanical and air flow properties. The design parameters were systematically adjusted to evaluate their performance during mechanical compression and airflow resistivity tests. For compression testing, we created cubic lattice structures with thicknesses of 0.3 mm, 0.4 mm, and 0.6 mm, and unit cell sizes of 4×4×4 mm, 6×6×6 mm, and 8×8×8 mm, all contained within a 30×30×30 mm cube. In contrast, cylindrical lattice structures were

fabricated for airflow resistivity tests, featuring a 32×32 mm dimension, 10×10 mm unit cell size, and a wall thickness of 0.80 mm. All lattice geometries were generated using Creo implicit modeling software, which allowed for precise parameter control based on the implicit mathematical functions governing each TPMS structure. Detailed Design parameters for various lattice structures are comprehensively presented in Table 1.

Table 1. Detailed Design parameters for various lattice structures

Structure Type	Component Code's	Cube Diamension (mm)	Unit Cell Size (mm)	Thickness (mm)	Structure View
GYROID	G1A	30X30X30	4X4X4	0.3	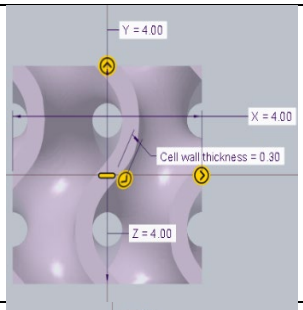
	G1B			0.4	
	G1C			0.5	
	G2A		6X6X6	0.3	
	G2B			0.4	
	G2C			0.5	
	G3A		8X8X8	0.3	
	G3B			0.4	
	G3C			0.5	
DIAMOND	D1A	30X30X30	4X4X4	0.3	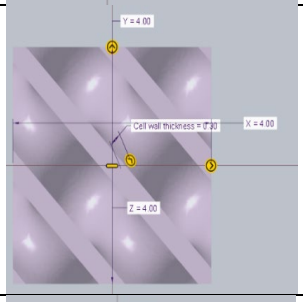
	D1B			0.4	
	D1C			0.5	
	D2A		6X6X6	0.3	
	D2B			0.4	
	D2C			0.5	
	D3A		8X8X8	0.3	
	D3B			0.4	
	D3C			0.5	
PRIMITIVE	P1A	30X30X30	4X4X4	0.3	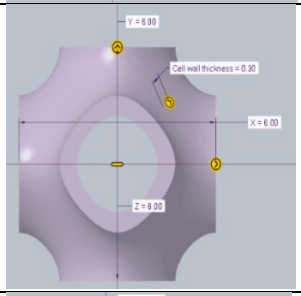
	P1B			0.4	
	P1C			0.5	
	P2A		6X6X6	0.3	
	P2B			0.4	
	P2C			0.5	
	P3A		8X8X8	0.3	
	P3B			0.4	
	P3C			0.5	
I-WP	I1A	30X30X30	4X4X4	0.3	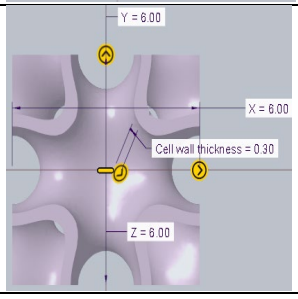
	I1B			0.4	
	I1C			0.5	
	I2A		6X6X6	0.3	
	I2B			0.4	
	I2C			0.5	
	I3A		8X8X8	0.3	
	I3B			0.4	
	I3C			0.5	

Figure 4 offers a detailed summary of different lattice structures, highlighting their unique measurements and properties. Each entry in the database consists of the type of structure, the codes assigned to its components, the dimensions of the cubes, the size of the cells, and the thickness measurements. This comprehensive presentation provides a thorough understanding of the various configurations and design possibilities for the lattice structures. By

analyzing these factors, one can gain a deeper understanding of how each design can fulfill specific functional needs and applications in engineering and manufacturing

Air Flow Resistivity Experimentation

The experimental setup for measuring the airflow resistivity of porous materials is carefully constructed to adhere to the ISO 9053-1:2018(E) standard, which provides detailed guidelines for evaluating static airflow resistance in a laminar flow environment. At the core of this system is a PVC pipe, measuring 60 mm in diameter, 5 mm in thickness, and 70 cm in length, which ensures a regulated airflow within the controlled environment. The airflow is produced by a 12 v cpu cooling fan that can rotate at speeds ranging from 6800 to 13000 rpm, enabling users to fine-tune the flow rates according to their specific requirements. The amprobe-tma5 mini vane anemometer is used to measure airflow velocity and the pressure drops across the material sample, ensuring accuracy within a range of ±5%. This arrangement allows for the examination of different porous materials under three predetermined airflow rates (3.3, 3.0, and 2.7 m/s), enabling the calculation of airflow resistivity using the collected data. Here is the experimental setup used in the test. The following setup shown in Figure 1, describes air flow resistivity experimental setup in the research article

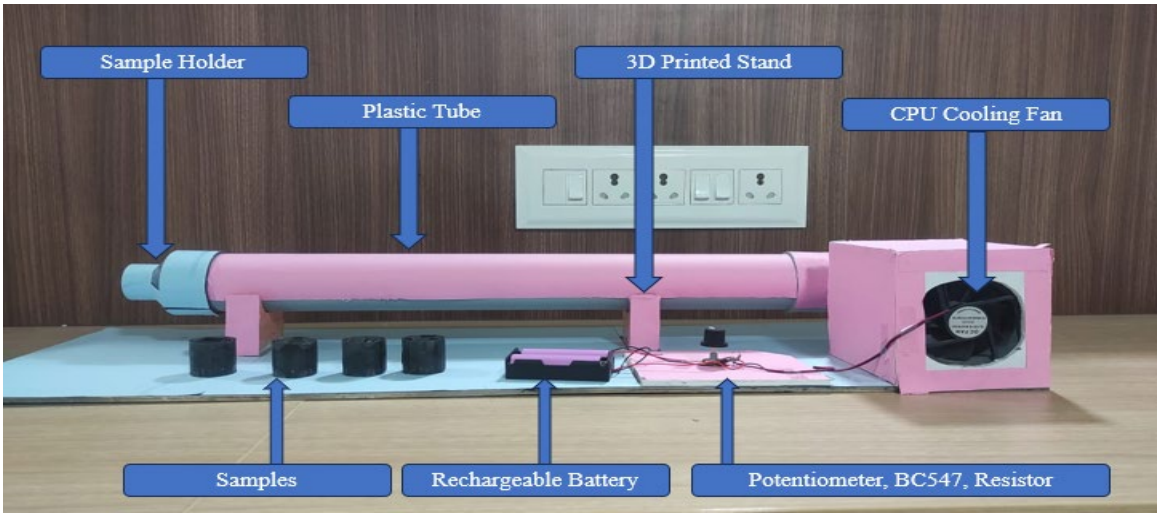

Figure 1. Air Flow Resistivity experimental setup.

The tube experiences low airflow due to the operation of the CPU fan. To ensure accurate testing, three airflow rates 3.3, 3.0, and 2.7 m/s were chosen to guarantee laminar flow within the setup. The initial step in the procedure involves assessing the airflow at the end of the sample holder, without any material present. Each sample is carefully positioned within the holder, and the airflow readings are recorded for each individual sample. Each sample is assessed at the three designated airflow rates. These data points are then utilized to determine pressure drop and flow resistivity. In cases where the airflow values remain relatively constant, each sample is tested ten times, and the average value is determined to ensure consistency. This entire process is repeated for each sample, and the final average airflow value is calculated. The core principle of this approach is to quantify the pressure difference between the two sides of the specimen as it is exposed to a regulated, one-way airflow.

Mechanical Testing

The compression testing of gyroid diamond primitive and inverse gyroid (I-WP) lattice structures was carried out in compliance with the ASTM D695 standard, which outlines the procedure for determining the compressive strength of rigid plastics. The testing was conducted using a mechanical testing machine, specifically an INSTRON 8801 system with a load capacity of 100 KN. Samples were created using additive manufacturing, guaranteeing consistency and accuracy in lattice structures. The samples were placed between two parallel plates, with the lower plate securely fixed to ensure stability during the testing process. The lattices were positioned on the compression plate in the same direction as their intended use to mimic real-life situations. The compression rate was maintained at a steady 2 mm/min, enabling precise monitoring of stress and strain until the structure deformed by 40% or the applied force reached 10 KN. By employing this approach, a comprehensive assessment of the mechanical behavior, including failure mechanisms and deformation patterns, could be conducted for both the gyroid diamond primitive and I-WP

lattices, offering valuable insights into their performance when subjected to compressive loads. The following setup, shown in Figure 2, describes the mechanical testing experimental setup in the research article.

Figure 2. Mechanical Testing Experimental Setup

4. Results and Discussion

The airflow resistivity test results for the four TPMs lattice structures, like gyroid, diamond, primitive, and I-WP, are examined to assess their performance under different airflow conditions. The test evaluates the resistance of the lattice structures to airflow, which is crucial for thermal management applications like battery packs or heat exchangers. The findings are displayed in three sets, each representing a different constant and varying airflow velocities.

a) 3.3 (m/sec)

The initial test was conducted without the lattice structure, then the velocity is 3.3 m/sec. Then we conducted the air flow resistivity test with different lattice structures. Table 2 presents the measured airflow resistivity values.

Table 2. Test result for 3.3 (m/sec)

Sr.no	Specimen	Constant value (m/sec)	Varying Value (m/sec)	Difference (%)
1	Gyroid	3.3	2	39.39
2	Diamond	3.3	1.5	54.55
3	Primitive	3.3	2	39.39
4	I-WP	3.3	2.1	36.36

b) 3.0 (m/sec)

An initial test was conducted without the lattice structure, then the velocity was 3.0 m/sec. Then we conducted the air flow resistivity test with different lattice structures. Table 3 presents the measured airflow resistivity values.

Table 3. Test result for 3.0 (m/sec)

Sr.no	Specimen	Constant value (m/sec)	Varying Value (m/sec)	Difference (%)
1	Gyroid	3	1.6	46.67
2	Diamond	3	1.3	65.67
3	Primitive	3	1.9	36.67
4	I-WP	3	1.9	36.67

c) 2.7 (m/sec)

An initial test was conducted without the lattice structure, then the velocity is 2.7 m/sec. Then we conducted the air flow resistivity test with different lattice structures. Table 4 presents the measured airflow resistivity values.

Table 4. Test result for 2.7 (m/sec)

Sr.no	Specimen	Constant value (m/sec)	Varying Value (m/sec)	Difference (%)
1	Gyroid	2.7	1.3	51.85
2	Diamond	2.7	1.1	59.26
3	Primitive	2.7	1.7	37.04
4	I-WP	2.7	1.6	40.74

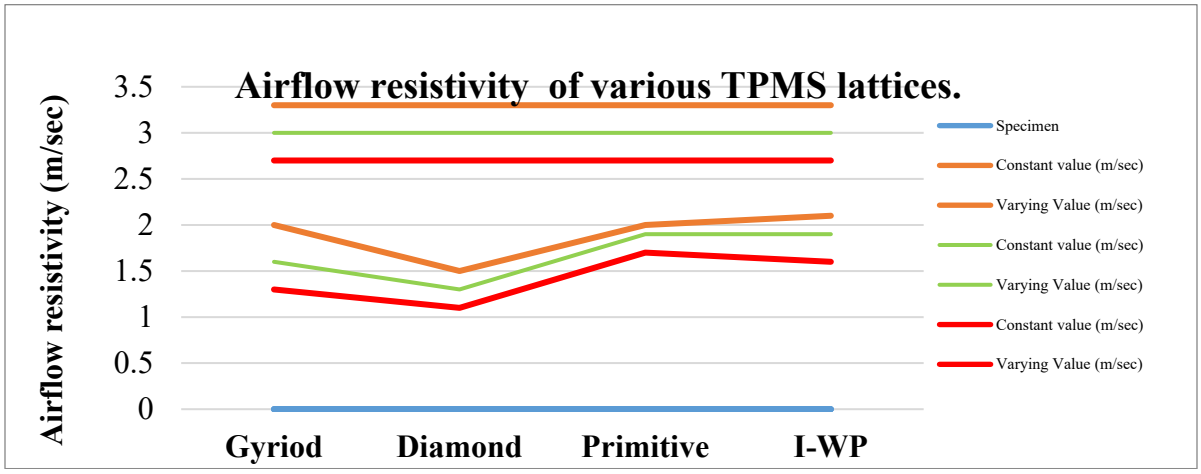

Figure 3. Comparative airflow resistivity measurements

Figure 3 presents comparative airflow resistivity measurements for all TPMS structures at varying flow velocities. Gyroid lattices demonstrated moderate airflow resistivity, ranging from 1.3 m/sec to 2 m/sec, with higher resistivity observed at elevated velocities (2 m/sec at 3.3 m/sec), indicating sensitivity to airflow changes. The surfaces of these interconnected components possess a harmonious balance of thermal conductivity and mechanical stability, making them ideal for various applications that demand these characteristics. In contrast, diamond lattices exhibited the lowest

airflow resistivity (1.1 m/sec to 1.5 m/sec), maintaining efficiency even at higher velocities, making them ideal for thermal management systems where minimal resistance is crucial. Primitive lattices delivered intermediate performance (1.7 m/sec to 2 m/sec), with increased resistivity at higher speeds due to their robust cellular framework, making them suitable for applications that require a balance between thermal management and structural integrity. Lastly, I-wp lattices exhibited slightly higher resistivity (1.6 m/sec to 2.1 m/sec) than diamond and primitive structures, as their double-curved surfaces led to localized stress concentrations. They are suitable for applications that require a moderate level of thermal conductivity and energy absorption. To visually depict the airflow resistivity of gyroid, diamond, primitive, and I-wp lattice structures, a line or bar graph can be constructed using the provided data points. The diagram provided above will facilitate a clearer comprehension of airflow patterns.

Mechanical Testing

The results from the compression tests reveal significant variations in the performance of the different lattice types, highlighting the importance of geometric design in optimizing mechanical properties. Each category exhibited unique load-bearing capabilities and compressive strengths, which were influenced not only by their intrinsic structural characteristics but also by the specific parameters of its design. This analysis lays the groundwork for understanding how bio-inspired lattices can be tailored for various applications in engineering and materials science. The comprehensive analysis of the compression test results for the bio-inspired lattice specimens is detailed in the following table, which lists each specimen label alongside its corresponding compressive strength (in MPa) and maximum compressive load in N). This tabulated data provides valuable quantitative insights into the mechanical performance of each lattice type, allowing for a clearer comparison between the gyroid, diamond, primitive, and I-wp structures. The results serve as a foundation for understanding the relationship between geometric parameters and mechanical properties, facilitating informed discussions regarding their design and application in various engineering contexts. Table 5 clearly shows the results for each TPMS configuration under compressive loading

Table 5. Compression Test Results of Bio-Inspired Lattice Specimens

Speci--men label	Compressive Strength (MPa)	Maximum Comp. load (N)	Speci--men label	Compressive Strength (MPa)	Maximum Comp. load (N)	Speci -men label	Compressive Strength (MPa)	Maximum Comp. load (N)
G1A	1.80814	1627.32605	P1B	2.19712	1977.4079	P1C	3.94262	3548.3598
`G2A	1.33681	1203.13171	P2B	1.72500	1552.49829	P2C	2.00525	1804.72131
G3A	0.95483	859.34399	P3B	1.08544	976.89630	P3C	2.07869	1870.82288
P1A	1.25851	1132.65515	I1B	4.06280	3656.51855	I1C	4.39960	3959.63794
P2A	0.70923	638.30615	I2B	1.51436	1362.92578	I2C	3.26623	2939.61157
P3A	0.79371	714.33783	I3B	1.87609	1688.48035	I3C	2.53594	2282.34521
I1A	0.95321	857.88965	G1C	3.53509	3181.57666	D1B	3.28926	2960.33618
I2A	1.43892	1295.02417	G2C	2.73660	2462.93555	D2B	3.22160	2899.43823
I3A	1.14289	1028.60327	G3C	1.96876	1771.88513	D3B	0.76855	691.69403
D1A	2.36641	2129.76929	D1C	7.61363	6852.26318	G1B	1.78856	1609.70093
D2A	1.62684	1464.15833	D2C	3.33560	3002.04150	G2B	1.30829	1177.45996
D3A	1.90955	1718.59265	D3C	1.37485	1237.36267	G3B	1.40288	1262.59326

The compression test outcomes demonstrate that the mechanical behavior of lattice structures is greatly affected by structural parameters like cell size and wall thickness. Specimens D1C and I1B, with greater wall thickness and optimized cell configurations, achieved impressive compressive strengths of 7.61 MPa and 4.06 MPa, respectively, along with maximum load capacities of 6852.26 N and 3656.52 N. In contrast, specimens P2A and D3B, characterized

by thinner walls and larger cell sizes, exhibited much lower compressive strengths of 0.709 MPa and 0.768 MPa and reduced load-bearing capacities of 638.31 N and 691.69 N. These findings strongly emphasize the significant impact of geometric parameters on the mechanical performance of TPMS-based lattice structures when subjected to compressive forces. I have printed a total of 36 samples, each representing a different compression structure, namely the gyroid, diamond, primitive, and I-WP lattice. Each graph combines nine specimens to offer a comprehensive visual representation of the compression capabilities of each lattice type. This organization enables a comprehensive examination of how each structure reacts to compressive forces, emphasizing differences in mechanical strength and deformation patterns. By presenting the results in this manner, it aimed to facilitate a straightforward comparison between the different lattice designs, enabling a better understanding of their structural integrity and potential applications in load-bearing scenarios. The additional graphs referenced in these further graphs are intended to bolster the credibility of the findings and facilitate informed decision-making in the selection of materials and engineering applications. Figure 4 clearly shows the distinct stress-strain curves for each TPMS configuration under compressive loading.

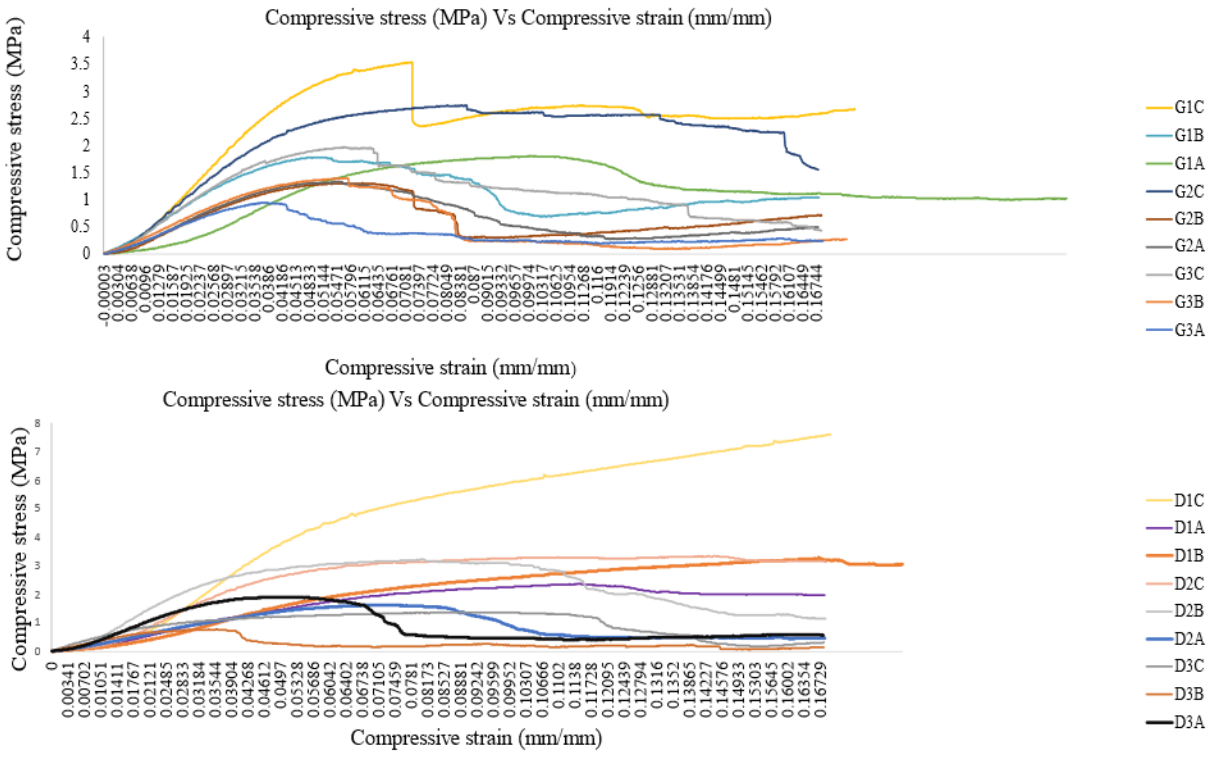

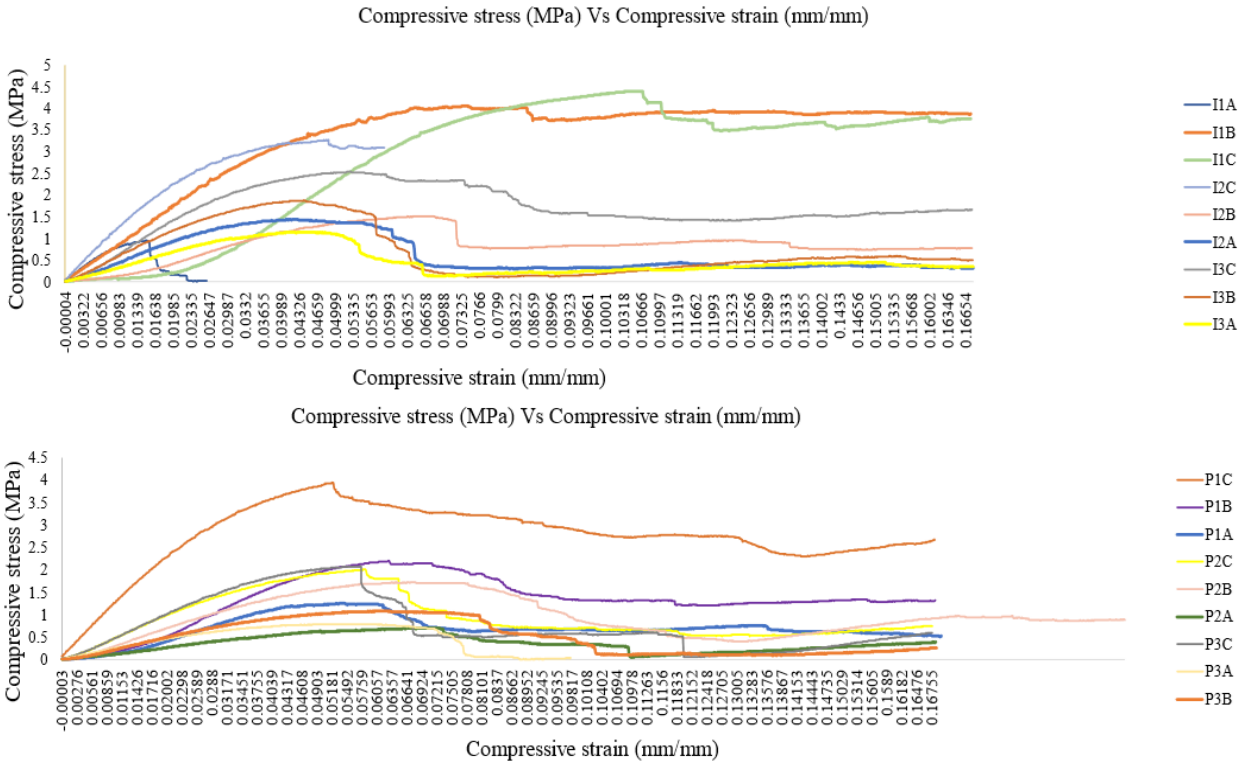

Figure 4. Illustrations of stress–strain diagrams of the different TPMS lattice structures

Gyroid structures. The specimens with gyroid lattice structures exhibited moderate compressive strength because their surfaces were interconnected smoothly, ensuring even stress distribution throughout the lattice network. The compressive strengths of the materials varied from 0.95 MPa to 3.35 MPa, with the highest compressive loads reaching between 959.34 N and 3181.57 N. Diamond structures. Diamond lattices demonstrated the highest overall performance among all tested structures, with compressive strengths ranging from 1.37 MPa to 7.16 MPa and maximum compressive loads between 1217.36 N and 6852.26 N. Primitive formations. Primitive lattice specimens displayed a balance between mechanical stiffness and deformation resistance, with compressive strengths ranging from 0.79 MPa to 3.94 MPa and maximum compressive loads between 714.37 N and 2840.73 N. I-WP structures. The I-WP lattice specimens exhibited a moderate level of mechanical performance, displaying compressive strengths between 0.85 MPa and 4.39 MPa, and maximum compressive loads between 857.89 N and 2999.63 N. The compression tests provided valuable information about how the lattice structures behaved when subjected to compressive forces. The average compressive strength across all specimens was determined to be 2.20366 MPa, suggesting a satisfactory overall performance. The highest compressive load values varied from 859.34 N (specimen G3A) to 6852.26 N (specimen D1C), demonstrating substantial differences influenced by lattice type, cell size, and wall thickness

These statistics highlight the wide range of mechanical performance across the specimens, driven by differences in lattice structure type, cell size, and wall thickness. The mean compressive strength is 2.20366 MPa, with values ranging from 0.79 MPa to 7.16 MPa. The highest compressive strength was observed in specimen D1C (Diamond structure, small cell size, thick walls). The lowest compressive strength was observed in specimen P3A (Primitive structure, large cell size, thin walls).

6. Conclusions

The airflow resistivity test results highlighted the thermal management capabilities of the four TPMS lattice structures under varying airflow velocities (2.7 m/sec, 3.0 m/sec, and 3.3 m/sec). The following conclusions were drawn:

1. Diamond Structures consistently exhibited the lowest airflow resistivity (ranging from 1.1 m/sec to 1.5 m/sec) due to their efficient airflow pathways, making them ideal for applications requiring high convective cooling efficiency.

2. Gyroid Structures showed moderate resistivity values (1.3 m/sec to 2 m/sec) due to their smooth periodic surfaces, balancing thermal conductivity with mechanical stability.
3. Primitive Structures displayed intermediate resistivity (1.7 m/sec to 2 m/sec) and are suitable for applications requiring a compromise between airflow efficiency and structural integrity.
4. I-WP Structures exhibited slightly higher resistivity (1.6 m/sec to 2.1 m/sec) due to their double-curved surfaces, but remain effective for moderate thermal management applications.

The results highlight that smaller cell sizes and efficient geometries contribute to reduced airflow resistivity, while larger voids increase turbulence.

The compression test results for the 36 specimens of bio-inspired lattice structures (Gyroid, Diamond, Primitive, and I-WP) revealed significant differences in mechanical performance based on lattice type, cell size, and wall thickness. The following conclusions can be drawn.

1. Diamond Structures demonstrated the highest compressive strength (up to 7.16 MPa) due to their robust interconnected framework, making them ideal for load-bearing applications requiring superior stiffness and energy absorption.
2. Gyroid Structures exhibited moderate compressive strength (ranging from 0.95 MPa to 3.35 MPa) and balanced performance, suitable for lightweight applications requiring moderate load-bearing capacity and energy absorption.
3. Primitive Structures offered a balance between stiffness and deformation resistance, with compressive strengths up to 3.94 MPa, making them versatile for lightweight structural designs.
4. I-WP Structures demonstrated intermediate mechanical properties (compressive strength ranging from 0.85 MPa to 4.39 MPa) and are suitable for energy absorption applications requiring moderate stiffness.

References

Al-Ketan, O., and Abu Al-Rub, R. K. (2019). Multifunctional mechanical metamaterials based on triply periodic minimal surface lattices: A review. Advanced Engineering Materials, 21(10), 1900524. https://doi.org/10.1002/adem.201900524

Al-Ketan, O., Rowshan, R., and Abu Al-Rub, R. K. (2017). Topology–mechanical property relationship of 3D printed strut, skeletal, and sheet-based periodic metallic cellular materials. Additive Manufacturing, 19, 167–183. https://doi.org/10.1016/j.addma.2017.12.006

Catchpole-Smith, S., Aboulkhair, N., Clare, A., and Tuck, C. (2019). Thermal conductivity of TPMS lattice structures manufactured via laser powder bed fusion. Additive Manufacturing, 30, 100846. https://doi.org/10.1016/j.addma.2019.100846

Karcher, H. (1989). The triply periodic minimal surfaces of Alan Schoen and their constant mean curvature companions. Manuscript Mathematica, 64(3), 291–357. https://doi.org/10.1007/BF01165824

Poltue, T., Karuna, C., Khrueaduangkham, S., Seehanam, S., and Promoppatum, P. (2021). Design exploration of 3D-printed triply periodic minimal surface scaffolds for bone implants. International Journal of Mechanical Sciences, 211, 106762. https://doi.org/10.1016/j.ijmecsci.2021.106762

Schoen, A. H. (1970). Infinite periodic minimal surfaces without self-intersections. NASA Technical Note D-5541.

Schwarz, H. A. (1865). On those cases in which the Gaussian hypergeometric series represents an algebraic function of its fourth parameter**.** Journal for Pure and Applied Mathematics*,* 75, 292–335.

Sun, Q., Sun, J., Guo, K., and Wang, L. (2022). Compressive mechanical properties and energy absorption characteristics of SLM fabricated Ti-6Al-4V triply periodic minimal surface cellular structures. Mechanics of Materials, 166, 104241. https://doi.org/10.1016/j.mechmat.2022.104241

Zhang, L., Feih, S., Daynes, S., Chang, S., Wang, M. Y., Wei, J., and Lu, W. F. (2018). Energy absorption characteristics of metallic triply periodic minimal surface sheet structures under compressive loading. Additive Manufacturing, 23, 505–515. https://doi.org/10.1016/j.addma.2018.08.007